Journal of Operation and Automation in Power Engineering
Vol. 2, No. 1, Winter & Spring 2014, Pages: 60-73
http://joape.uma.ac.ir

Combined Use of Sensitivity Analysis and Hybrid Wavelet-PSO-ANFIS to Improve Dynamic Performance of DFIG-Based Wind Generation

M. Darabian*, A. Jalilvand, R. Noroozian
Department of Electrical Engineering, University of Zanjan, Zanjan, Iran

ABSTRACT
In the past few decades, increasing growth of wind power plants causes different problems for the power quality in the grid. Normal and transient impacts of these units on the power grid clearly indicate the need to improve the quality of the electricity generated by them in the design of such systems. Improving the efficiency of the large-scale wind system is dependent on the control parameters. The main contribution of this study is to propose a sensitivity analysis approach integrated with a novel hybrid approach combining wavelet transform, particle swarm optimization and an Adaptive-Network-based Fuzzy Inference System (ANFIS) known as Wavelet-ANFIS-PSO to acquire the optimal control of Doubly-Fed Induction Generators (DFIG) based wind generation. In order to mitigate the optimization complexity, sensitivity analysis is offered to identify the Unified Dominate Control Parameters (UDCP) rather than optimization of all parameters. The robustness of the proposed approach in finding optimal parameters, and consequently achieve a high dynamic performance is confirmed on two area power system under different operating conditions.

KEYWORDS: Doubly fed induction generator, Fuzzy logic, Neural networks, Particle Swarm Optimization, Wavelet transform, Sensitivity analysis.

NOMENCLATURE

ψ_{dr}	The d axis rotor flux linkages
ψ_{qr}	The q axis rotor flux linkages
L_{ss}	The stator self-inductance
L_{rr}	The rotor self-inductance
L_m	The mutual inductance
R_r	The rotor resistance
ω_s	The synchronous angle speed
S_r	The rotor slip
X_s	The stator reactance
X'_s	The stator transient reactance
E'_d	The d axis voltage behind the transient reactance
E'_q	The q axis voltage behind the transient reactance
T'_o	The rotor circuit time constant
i_{ds}	The d axis stator current
i_{qs}	The q axis stator current
v_{ds}	The d axis stator terminal voltages
v_{qs}	The q axis stator terminal voltages
v_{dr}	The d axis rotor terminal voltages
v_{qr}	The q axis rotor terminal voltages
ω_r	The generator rotor angle speed
ω_t	The wind turbine angle speed
H_g	The inertia constants of the generator
H_t	The inertia constants of the turbine
θ_{tw}	The shaft twist angle
K_{sh}	The shaft stiffness coefficient
D_{sh}	The damping coefficient
T_{sh}	The shaft torque
T_m	The wind torque
T_{em}	The electromagnetic torque
ρ	The air density
R	The wind turbine blade radius
V_ω	The wind speed
C_f	The blade design constant coefficient
β	The blade pitch angle
λ	The blade tip speed ratio
C_P	The power coefficient
P_s	The stator active power
P_r	The active power at the ac terminal of

Submission date : 16 Aug. 2013 Revised: 22 Sep. 2013
Acceptance date : 15 Nov. 2013
Corresponding author :
M. Darabian (E-mail: m.darabian@znu.ac.ir)

	the rotor side converter (RSC)
P_g	The active power at the ac terminal of the grid side converter (GSC)
P_{DC}	The active power of the dc link capacitor
i_{dr}	The d axis rotor currents
i_{qr}	The q axis rotor currents
i_{dg}	The axis currents of the GSC
i_{qg}	The axis currents of the GSC
V_{dg}	The d axis voltage of the GSC
v_{qg}	The q axis voltage of the GSC
V_{DC}	The dc link capacitor voltage
i_{DC}	The current of the dc link capacitor
C	The capacitance of the dc link capacitor
K_{p1}& K_{i1}	The PI gains of the power regulator
K_{p2}& K_{i2}	The PI gains of RSC Current regulator
K_{p3}& K_{i3}	the PI gains of the grid voltage regulator
i_{dr}^{ref}	The current control references for the d axis components of the GSC
i_{qr}^{ref}	The current control references for the q axis components of the GSC
Vs_{ref}	The specified terminal voltage reference
P_{ref}	The active power control reference
K_{pdg}& K_{idg}	the PI gains of the link dc capacitor voltage regulator
K_{pg}& K_{ig}	The PI gains of the grid side converter current regulator
v_{DCref}	The voltage control reference of the dc link capacitor
i_{qgref}	The control reference for the q axis component of the GSC current
K_{p4}& K_{i4}	The PI gains of the WT speed regulator
$\Delta\omega_t$	The deviation of the WT rotating speed

1. INTRODUCTION

Doubly Fed Induction Generator (DFIG) is a popular Wind Turbine (WT) system due to its various abilities such as high-energy efficiency; reduction in mechanical stress on wind turbine; reactive power control; reduction in convertor cost and injection of reactive power in the case of voltage oscillation to regulate terminal voltage [1]. A DFIG system, including induction generator, two mass drive trains, power converters, and feedback controllers, is a multivariable, nonlinear and strongly coupled system. Bifurcation phenomena in such a nonlinear system may occur under certain conditions, leading to oscillatory instability. Hence, practical analysis of DFIG stability will have to involve the bifurcation phenomena. In recent years, a number of researchers studied stability of industrial motor drives with a wealth of nonlinear dynamics according to the bifurcation and chaos theories [2, 3]. Wind speed characteristics of the potential wind farm site as well as governmental support are considered the most important criteria for constructing wind farm projects [4]. In most systems, however, there may be other parameters besides wind speed for optimal development of wind power from the system perspective, whereas there is an urgent need to priorities the construction of wind farm projects throughout the system. Moreover, in the current deregulated environment, there are fewer incentives for transmission system expansion, which causes increased network deficiency, and therefore less reliability [5, 6]. Hence, large-scale wind integration policy should also consider system reliability issues, particularly those related to transmission limitations. Wind power prediction is a primary requirement for efficient large-scale integration of wind generation in power systems and electricity markets [7-10]. The stability analysis and optimal control of wind turbine with DFIG have been studied by many researchers [11-15]. A PSO based approach is presented in [16] to optimize all the control parameters in a DFIG simultaneously in order to improve the performance of the DFIG in the power grid. However, increasing the number of the DFIG in a wind farm will lead to increase the number of the control parameters. The proposed Adaptive Dynamic Programming (ADP) based schemes in [17-20] have presented great success in such a multivariable area. Sensitivity analysis is one of the most significant schemes used in power system to analyze and model [21]. The robust sensitivity analysis and voltage sensitivity analysis are respectively applied to acquire the impact of different DFIG parameters on different critical pairs at different rotor speeds [22, 23]. The identification of a Uniformed Dominate Control Parameters (UDCP) is one of the most challenging problem to mitigate the optimization complexity in large-scale wind farms. For this purpose, this study proposes a novel hybrid approach, combining wavelet transform, particle swarm optimization, and an adaptive-network-based fuzzy Inference system

to attain the optimal control of DFIG. The sensitivity analysis is used to distinguish the critical parameters UDCP from all parameters and then the proposed strategy is applied to obtain optimal values to enhance dynamic characteristics. Simulation and comparative analysis reveal the robustness of the proposed method.

This paper is organized as follows: In Sec. 2 the power system model is described. The sensitivity analysis and DFIG Control parameters sensitivity analysis are drawn in Sec. 3 and 4, respectively. In Sec. 5, the UDCP Optimization using hybrid Wavelet-PSO-ANFIS approach is presented. Finally, Sec. 6 and 7 give simulation results and conclusions, respectively.

2. WT WITH DFIG MODEL

In this section the wind farm is presented by one WT with DFIG system. The configuration of the simulated single wind farm infinite bus system is depicted in Fig. 1. The wind turbine uses a DFIG consisting of a wound rotor induction generator and an ac/dc/ac Insulated-Gate Bipolar Transistor (IGBT) based Pulse Width Modulation (PWM) converter. In addition, the stator winding is connected directly to the 60 Hz grid while the rotor is fed at variable frequency through the ac/dc/ac converter [24, 25]. As shown in Fig. 2, the DFIG system utilizes a wound rotor induction generator in which the stator windings are directly connected to the three-phase grid and the rotor windings are fed through three-phase back-to-back bidirectional PWM converters. Also, the back-to-back PWM converter consists of three parts: a Rotor Side Converter (RSC), a Grid Side Converter (GSC) and a dc link capacitor placed between the two converters. For the rotor and grid-side converters, vector control strategy is used to acquire separate control of active and reactive power.

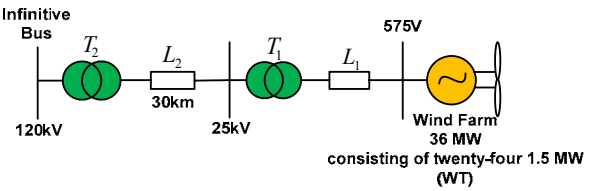

Fig. 1. The diagram of the power system including a DFIG-based wind farm.

2.1 Generator model

According to the voltage and flux-linkage equations of the induction generator [26,27], the differential equations of the stator and rotor circuits of the induction generator with stator and rotor currents as state variables can be given as follows:

$$\frac{X'_s}{\omega_s}\frac{d_{ids}}{dt} = v_{ds} - \left[R_s + \frac{(X_s - X'_s)}{\omega_s T'_0}\right] \times i_{ds} - (1 - s_r)E'_d$$
$$- \frac{L_m}{L_{rr}} v_{dr} \times \left(-\frac{1}{\omega_s T'_0}\right) E'_q - X'_s i_{qs} \quad (1)$$

$$\frac{X'_s}{\omega_s}\frac{d_{iqs}}{dt} = v_{qs} - \left[R_s + \frac{(X_s - X'_s)}{\omega_s T'_0}\right] \times i_{qs} - (1 - s_r)E'_q$$
$$- \frac{L_m}{L_{rr}} v_{qr} \times \left(-\frac{1}{\omega_s T'_0}\right) E'_d - X'_s i_{ds} \quad (2)$$

$$\frac{dE'_d}{dt} = s_r \omega_s E'_q - \omega_s \frac{L_m}{L_{rr}} v_{qr} - \frac{1}{T'_0} \times [E'_d + (X_s - X'_s) i_{ds}] \quad (3)$$

$$\frac{dE'_q}{dt} = s_r \omega_s E'_d - \omega_s \frac{L_m}{L_{rr}} v_{dr} - \frac{1}{T'_0} \times [E'_q + (X_s - X'_s) i_{qs}] \quad (4)$$

where,

$$E'_d = -(\omega_s \times \frac{L_m}{L_{rr}} \psi_{qr}),\ E'q = -(\omega_s \times \frac{L_m}{L_{rr}} \psi_{dr})$$

$$X_s = \omega_s \times L_{ss},\ X'_s = \omega_s \times \left[L_{ss} - \left(\frac{L_m^2}{L_{rr}}\right)\right],\ T'_0 = \frac{L_{rr}}{R_r}$$

2.2 Drive train model

A turbine, a low and a high speed shaft, and a gearbox are the main elements of the drive train system which can be expressed by following equations:

$$2H_t \frac{d\omega}{dt} = T_m - T_{sh} \quad (5)$$

$$\frac{d\theta_{t\omega}}{dt} = \omega_t - \omega_r = \omega_t - (1 - s_r)\omega_s \quad (6)$$

$$2H_g \frac{d_{sr}}{dt} = -T_{em} - T_{sh} \quad (7)$$

$$T_{sh} = K_{sh}\theta_{t\omega} + D_{sh}\frac{d\theta_{t\omega}}{dt} \quad (8)$$

where

$$T_m = \frac{0.5\rho\pi R^2 C_p V_\omega{}^3}{\omega_t} \quad (9)$$

$$T_{em} = \frac{P_s}{\omega_s} \quad (10)$$

C_p is given by:

$$C_p = \frac{1}{2}\left(\frac{RC_f}{\lambda} - 0.22\beta - 2\right) e^{\frac{-0.225RC_f}{\lambda}} \quad (11)$$

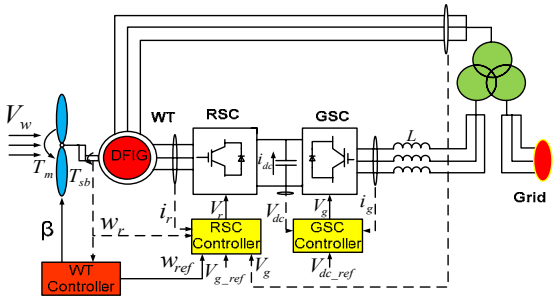

Fig. 2. The diagram of DFIG based wind turbine.

2.3 DC link capacitor model

DC link capacitor is responsible for balancing the active power flow through the back-to-back PWM converter (see Fig. 2) and can be stated as follow:

$$P_r = P_g + P_{DC} \tag{12}$$

where

$$P_r = v_{dr} i_{dr} + v_{qr} i_{qr} \tag{13}$$

$$P_g = v_{dg} i_{dg} + v_{qg} i_{qg} \tag{14}$$

$$P_{DC} = v_{DC} i_{DC} = -C v_{DC} \frac{dv_{dc}}{dt} \tag{15}$$

Substituting (13)-(15) into (12) we have:

$$C v_{DC} \frac{dv_{DC}}{dt} = v_{dg} i_{dg} + v_{qg} i_{qg} - (v_{dr} i_{dr} + v_{qr} i_{qr}) \tag{16}$$

2.4 Rotor Side Controller model

The schematic diagram of RSC is shown in Fig. 3. In this case, the active power and voltage are controlled independently via v_{qr} and v_{dr}, respectively which can be expressed as follows:

$$\frac{dx_1}{dt} = P_{ref} + P_s \tag{17}$$

$$i_{q-ref} = K_{p1}(P_{ref} + P_s) + K_{i1} x_1 \tag{18}$$

$$\frac{dx_2}{dt} = i_{q-ref} - i_{qr} = K_{p1}(P_{ref} + P_s) + K_{i1} x_1 - i_{qr} \tag{19}$$

$$\frac{dx_3}{dt} = v_{s-ref} - v_s \tag{20}$$

$$i_{d-ref} = K_{p3}(v_{s-ref} - v_s) + K_{i3} x_3 \tag{21}$$

$$\frac{dx_4}{dt} = i_{d-ref} - i_{dr} = K_{p3}(v_{s-ref} - v_s) + K i_3 x_3 - i_{dr} \tag{22}$$

$$v_{qr} = K_{p2}(K_{p1}\Delta P + K_{i1} x_1 - i_{qr}) + K i_2 x_2 + s_r \omega_s L_m i_{ds} + s_r \omega_s L_{rr} i_{qr} \tag{23}$$

$$v_{dr} = K_{p2}(K_{p3}\Delta U + K i_3 x_3 - i_{dr}) + K i_2 x_4 - s_r \omega_s L_m i_{qs} - s_r \omega_s L_{rr} i_{dr} \tag{24}$$

2.5 Grid Side Controller (GSC) model

The schematic diagram of GSC is illustrated in Fig. 4. The GSC has a duty to maintain the dc link voltage and control the terminal reactive power. The reactive power and dc link voltage are controlled independently via *iqg* and *idg*, respectively which can be expressed as follows:

$$\frac{dx_5}{dt} = v_{DC-ref} - v_{DC} \tag{25}$$

$$i_{dg-ref} = -K_{pdg}\Delta v_{DC} + K_{idg} x_5 \tag{26}$$

$$\frac{dx_6}{dt} = i_{dg-ref} - i_{dg} = -K_{pdg}\Delta v_{DC} + K i_{dg} x_5 - i_{dg} \tag{27}$$

$$\frac{dx_7}{dt} = v_{qg-ref} - iqg \tag{28}$$

$$\Delta v_{dg} = K_{pg}\frac{dx_6}{dt} + K_{ig} x_6 = K_{pg}(-K_{pdg}\Delta v_{DC} + K i_{dg} x_5 - i_{dg}) + K i_g x_6 \tag{29}$$

$$\Delta v_{qg} = K_{pg}\frac{dx_7}{dt} + K i_g x_7 = K_{pg}(i_{qg-ref} - i_{qg}) + K i_g x_6 \tag{30}$$

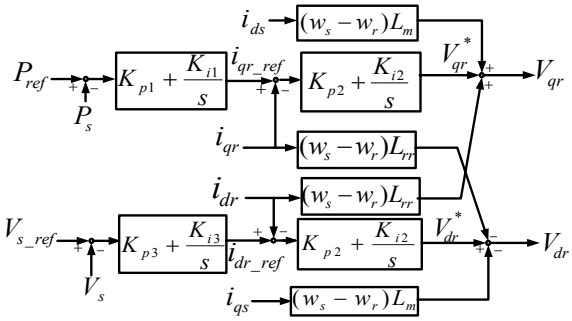

Fig. 3. Schematic diagram of RSC.

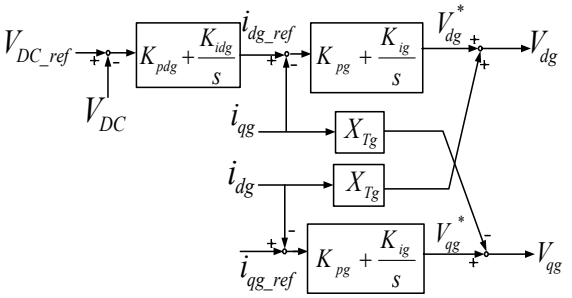

Fig. 4. Schematic diagram of GSC.

2.6 Pitch Controller (PC) model

The schematic diagram of PC is depicted in Fig. 5. The power extraction of WT as well as preventing overrated power production in strong wind are optimized by the pitch angle control which can be modeled as follows:

$$\frac{d\beta}{dt} = K_{p4} - \frac{T_m - T_{sh}}{2H_t} + K_{i4}\Delta\omega_t \tag{31}$$

The control of electrical dynamics can be separated from that of mechanical dynamics due to being much faster than the mechanical dynamics. Therefore, in this paper, we set KP4=KP2 and Ki4=Ki2.

According to above-mentioned, the model of WT with DFIG system can be restated as follows:

$$\dot{X} = f(X,U) \tag{32}$$

Where, X and U are the vectors of the DFIG state variables and input variables defined as follows:

$$X = [\omega_t, \beta, \theta_{t\omega}, s_r, i_{ds}, i_{qs}, E'_d, E'_q, x_1, x_2, x_3, x_4, V_{DC}, x_5, x_6, x_7]^T \tag{33}$$

$$U = [v_{ds}, v_{qs}, i_{dg}, i_{qg}]^T \tag{34}$$

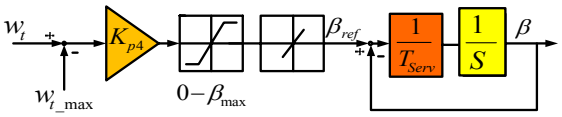

Fig. 5. Schematic diagram of pitch control.

3. SENSITIVITY ANALYSIS

3.1 Trajectory sensitivity analysis

The degree of change of the system when a parameter of the system subjects to small changes and it reflects the derivative relations between the system trajectory and the system parameters is evaluated by the sensitivity analysis which in turn diminish the complexity of simulation [28-29]. A power system applicable sensitivity analysis, is given by the following equation:

$$\begin{cases} \dfrac{dx}{dt} = f(x,y,\theta) \\ 0 = g(x,y,\theta) \\ x(t_0) = x_0 \\ y(t_0) = y_0 \end{cases} \tag{35}$$

Where x is the system state variables, y is the system output variables and θ is the control parameters. The Sensitivity of the control parameters evaluated by the trajectory can be expressed by data from time domain simulations as follows:

$$\frac{\partial y_i(\theta,k)}{\partial \theta_j} = \lim_{\Delta\theta_j \to 0} \frac{y_{i(\theta_1,..\theta_j+\Delta\theta_j,..\theta_m,k)} - y_i(\theta_1,...\theta_j,...,\theta_m\theta_k)}{\Delta\theta_j} \tag{36}$$

Where v_i is the trajectory curve of the *ith* variable and corresponds to the *jth* control parameter, m is the total number of control parameters, k is the time instance, and $\Delta\theta_j$ is the change of the parameter of θ. In order to avoid the deflection error and improve the accuracy of the numerical calculation, the system trajectory is needed to calculate twice, by either increment or decrement of a $\Delta\theta_j$:

$$\begin{cases} y_i(\theta_1,...,\theta_j+\Delta\theta_j,...,\theta_m,k) \\ y_i(\theta_1,...,\theta_j-\Delta\theta_j,...,\theta_m,k) \end{cases} \tag{37}$$

Then the relative value of the group of trajectory sensitivity can be calculated as:

$$\frac{\partial\left[\frac{y_i(\theta,k)}{y_{i0}}\right]}{\partial\left[\frac{\theta_j}{\theta_{jo}}\right]} = \frac{\frac{[y_i(\theta_1,...,\theta_j+\Delta\theta_j,...,\theta_m,k)-y_i(\theta_1,...,\theta_j-\Delta\theta_j,...,\theta_m,k)]}{y_{i0}}}{\frac{2\Delta\theta_j}{\theta_{j0}}} \tag{38}$$

where, θ_{jo} is the given value of parameter θ_j and y_{io} is the corresponding steady-state value given θ_{jo}. The mean trajectory sensitivity in order to compare the sensitivity value of these different control parameters can be calculated as follows:

$$A_{ij} = \frac{1}{K}\sum_{k=1}^{k}\left|\frac{\partial[\frac{y_i(\theta,k)}{y_{i0}}]}{\partial[\frac{\theta_j}{\theta_{j0}}]}\right| \tag{39}$$

where, k is the number of samples on the trajectory sensitivity curves.

3.2 Eigenvalue sensitivity analysis

The power system state equation is obtained by linearizing (35) as follow:

$$\dot{X} = AX \tag{40}$$

Where A is the Jacobian matrix of the system. Then the characteristic equation of the system is:

$$|\lambda I - A| = 0 \tag{41}$$

where, I is an unit matrix with same dimension as A. Therefore, the system eigenvalues $\lambda_1, \lambda_2, \ldots, \lambda_n$ are obtained via (41). The Jacobin matrix is a function of the control parameter *(A(θ))*. Then each eigenvalue λ_i of $A(\theta)$ will be the function of θ *($\lambda_i(\theta)$)*. Therefore, the sensitivity of eigenvalue λ_i to the control parameter θ is defined as follows:

$$\frac{\partial\lambda_{i\theta}}{\partial\theta_j} = v_i^T \frac{\partial A(\theta)}{\partial\theta_j} u_j \tag{42}$$

where, u and v are right and left eigenvector, respectively.

4. DFIG CONTROL PARAMETERS SENSITIVITY ANALYSIS

4.1 DFIG control parameters trajectory sensitivity analysis

According to the model of the system shown in Fig.1, a three phase ground fault with the fault resistance 20 Ω in each phase which starts at 15 sec and last for 0.15 sec is located at the Bus-25 KV. The active power trajectory of the DFIG is chosen as the object function in this paper. The active power of DFIG under the fault condition is shown in Fig. 6. The procedure of trajectory sensitivity analysis is as follows:

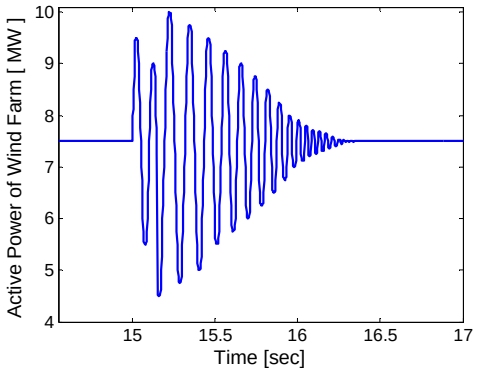

Fig. 6. Active power of WT with DFIG.

a) Consider the parameters for the controller of the WT system are: K_{p1}, K_{i1}, K_{p2}, K_{i2}, K_{p3}, K_{i3}, K_{pdg}, K_{idg}, K_{pg}, K_{ig}. Increase the value of these control parameters 10%, and acquire the trajectory of DFIG active power.

b) Decrease the value of these control parameters 10%, and acquire the trajectory of DFIG active power.

c) Compute the trajectory sensitivity of each control parameter through equation (39).

The sensitivities of the control parameters and their classification are tabulated in Table 1. K_{i3} and K_{pg} with trajectory sensitivity value of 2.1213 and 0.0016 are the largest one and smallest one, respectively (see Table 1). Hence K_{i3} and K_{p1} are assumed as the dominate control parameters for the trajectory sensitivity analysis.

4.2 DFIG control parameters eigenvalue sensitivity analysis

As previously mentioned, the system state vector is defined as follows:

$$X=[\omega_t,\beta,\theta_{t\omega},s_r,i_{ds},i_{qs},E'_d,E'_q,x_1,x_2,x_3,x_4,V_{DC},x_5,x_6,x_7]^T \quad (43)$$

The system eigenvalues and participation factors given by small signal stability analysis are shown in Table 2. Ignoring the stator transients, the state vector can be rewritten as follows:

$$X=[\omega_t,\beta,\theta_{t\omega},s_r,E'_d,E'_q,x_1,x_2,x_3,x_4,V_{DC},x_5,x_6,x_7]^T \quad (44)$$

Table 1. Sensitivity and classification of each control parameters.

Parameters	Sensitivity Value	Order		
		1	2	3
K_{p1}	1.1422	√	-	-
K_{i1}	0.108	-	√	-
K_{p2}	0.5986	-	√	-
K_{i2}	0.0854	-	√	-
K_{p3}	0.4863	-	√	-
K_{i3}	2.1213	√	-	-
K_{pdg}	0.0396	-	-	√
K_{idg}	0.00632	-	-	√
K_{pg}	0.0016	-	-	√
K_{ig}	0.0366	-	-	√

Table 2. System eigenvalue and participation factors analysis.

λ	σ	ω	f	ASV_1	ASV_2
λ_1	-1256	0	0	V_{DC}	-
λ_2	-176.2	0	0	x_5	x_6
$\lambda_{3,4}$	-69.8	112.3	17.8	E'_q	x_3
$\lambda_{5,6}$	-94.7	44.3	7.4	E'_d	x_1
$\lambda_{7,8}$	-2.86	60.4	0.91	$\theta_{t\omega}$	S_r
λ_9	-76.01	0	0	E'_d	x_1
$\lambda_{10,11}$	-0.56	0.69	0.116	ω_t	β
λ_{12}	-15.12	0	0	x_5	x_6
λ_{13}	-24.9	0	0	x_4	-
λ_{14}	-24.35	0	0	x_2	-

The eigenvalue sensitivities of control parameters and the sorted array of their value are given in Table 3 and 4, respectively. As seen in the Tables, K_{pdg} and K_{pg} have the largest eigenvalue sensitivity in response to λ_1 compared to others (with the value of 34.8764 and 12.4459), and consequently are chosen to be the dominate control parameters. Furthermore, K_{i1} and K_{i2} are assumed as a dominate control parameter owing to dominate for most of the eigenvalue ($\lambda_{3,4}$, $\lambda_{5,6}$, $\lambda_{7,8}$, λ_9, $\lambda_{10,11}$, $\lambda_{13,14}$). Hence, the unified dominate control parameters are: K_{i3}, K_{p1}, K_{i1}, K_{i2}, K_{pdg}, K_{pg}.

5. HYBRID WAVELET-PSO-ANFIS APPROACH

The proposed approach is based on the combination of WT, PSO and ANFIS [1]. The WT is used to decompose the wind power series into a set of better-behaved constitutive series. Then, the future values of these constitutive series are estimated using ANFIS. The PSO is used to improve the performance of ANFIS. Three optimization options are used to verify the robustness of the proposed scheme:

a) Optimize all the control parameters (K_{p1}, K_{i1}, K_{p2}, K_{i2}, K_{p3}, K_{i3}, K_{pdg}, K_{idg}, K_{pg}, K_{ig}) simultaneously.

b) Optimize the six UDCP (K_{i3}, K_{p1}, K_{i1}, K_{i2}, K_{pdg}, K_{pg}), and the other control parameters are set as default value.

c) Optimize random six control parameters.

5.1 Wavelet Transform

The WT decomposes the wind power series into a set of better-behaved constitutive series. These constitutive series should be predicted more accurately owing to filtering effect of the WT. WTs could be divided in two categories: Continuous Wavelet Transform (CWT) and Discrete WT (DWT). The CWT $W(a,b)$ of signal $f(x)$ is defined as follow [30]:

$$W(a,b)=\frac{1}{\sqrt{a}}\int_{-\infty}^{+\infty} f(x)\phi\left(\frac{x-b}{a}\right)dx \qquad (45)$$

Where, $\Phi(x)$ is a mother wavelet, the scale parameter a controls the spread of the wavelet and translation parameter b determines its central position. DWT is defined as [31]:

$$W(m,n)=2^{-\left(m/2\right)}\sum_{t=0}^{T-1} f(t)\phi\left(\frac{t-n2^m}{2^m}\right) \qquad (46)$$

Where, T is the length of the signal $f(x)$.The scaling and translation parameters are functions of the integer variables m and n ($a=2^m$, $b=n2^m$) is the discrete time index. A multilevel decomposition process can be achieved by successive decomposition of the approximations, where the original signal is broken down into lower resolution components (see Fig. 7).

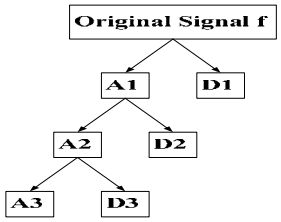

Fig. 7. Multilevel decomposition process.

Table 4. Classify the sensitivity of control parameters.

λ	Control parameters array by eigenvalue sensitivity
λ_1	$K_{pdg}>K_{pg}>K_{p2}>K_{ig}>K_{p1}>K_{p3}>K_{i2}>K_{i1}>K_{i3}>K_{idg}$
λ_2	$K_{ig}>K_{idg}>K_{pg}>K_{pdg}>K_{i2}>K_{p1}>K_{p2}>K_{i1}>K_{i3}>K_{p3}$
$\lambda_{3,4}$	$K_{i2}>K_{p2}>K_{i1}>K_{ig}>K_{p3}>K_{pg}>K_{p1}>K_{i3}>K_{idg}>K_{pdg}$
$\lambda_{5,6}$	$K_{i2}>K_{p2}>K_{i1}>K_{ig}>K_{p1}>K_{pg}>K_{i1}>K_{p3}>K_{idg}>K_{pdg}$
$\lambda_{7,8}$	$K_{i2}>K_{p2}>K_{i1}>K_{p1}>K_{ig}>K_{i3}>K_{pg}>K_{p3}>K_{idg}>K_{pdg}$
λ_9	$K_{i2}>K_{i1}>K_{p2}>K_{ig}>K_{p1}>K_{pg}>K_{i3}>K_{p3}>K_{idg}>K_{pdg}$
$\lambda_{10,11}$	$K_{i2}>K_{i1}>K_{p2}>K_{p1}>K_{ig}>K_{i3}>K_{pg}>K_{idg}>K_{p3}>K_{pdg}$
λ_{12}	$K_{idg}>K_{pdg}>K_{pg}>K_{ig}>K_{i2}>K_{i1}>K_{p2}>K_{p1}>K_{i3}>K_{p3}$
λ_{13}	$K_{i2}>K_{p2}>K_{i3}>K_{i1}>K_{ig}>K_{p3}>K_{p1}>K_{pg}>K_{idg}>K_{pdg}$
λ_{14}	$K_{i2}>K_{p2}>K_{i1}>K_{p1}>K_{i3}>K_{ig}>K_{p3}>K_{pg}>K_{idg}>K_{pdg}$

5.2 Particle Swarm Optimization

The PSO algorithm is based on the biological and sociological behavior of animals searching for their food [32-34]. Consider an optimization problem of D variables. A swarm of N particles is initialized in which each particle is assigned a random position in the D-dimensional hyperspace. Let x denote a particle's position and v denote the particle's flight velocity over a solution space. The best previous position of a particle is *Pbest*. The index of the best

Table 3. Sensitivity of control parameters to each eigenvalue

λ	K_{p1}	K_{i1}	K_{p2}	K_{i2}	K_{p3}	K_{i3}	K_{p1}	K_{idg}	K_{pg}	K_{ig}
λ_1	0.8594	0.0212	7.6912	0.1895	0.3354	0.0092	K_{i1}	0.0062	12.984	1.4163
λ_2	0.0055	0.0108	0.0465	0.0832	0.0062	0.0017	0.2295	0.5496	0.3125	20.026
$\lambda_{3,4}$	0.0281	0.0684	1.1201	2.6795	0.0694	0.1921	$6.74e^{-5}$	0.0016	0.0396	0.0954
$\lambda_{5,6}$	0.1545	0.4762	0.8977	2.598	0.0129	0.0976	0.0026	0.0018	0.1497	0.4752
$\lambda_{7,8}$	$7.85e^{-4}$	0.0046	0.0072	0.0362	$5.96e^{-6}$	$3.25e^{-5}$	$7.81e^{-8}$	$3.54e^{-7}$	$1.22e^{-5}$	$7.65e^{-5}$
λ_9	0.1298	0.5447	0.4203	1.7023	0.0035	0.0125	$6.25e^{-6}$	0.0001	0.0432	0.1729
$\lambda_{10,11}$	$3.91e^{-9}$	$1.24e^{-6}$	$3.55e^{-8}$	$1.16e^{-5}$	$6.2e^{-14}$	$2.12e^{-11}$	$1.11e^{-14}$	$3.28e^{-12}$	$4.94e^{-12}$	$1.15e^{-9}$
λ_{12}	$4.51e^{-8}$	$9.38e^{-7}$	$3.41e^{-7}$	$7.62e^{-6}$	$5.71e^{-10}$	$1.14e^{-8}$	0.0211	0.5496	0.0241	0.0122
λ_{13}	$3.66e^{-4}$	0.0034	0.2212	2.6852	0.0052	0.0061	$6.71e^{-8}$	$1.26e^{-6}$	$7.69e^{-5}$	0.0032
λ_{14}	0.0028	0.0368	0.1821	0.1862	0.0026	0.0024	$1.67e^{-6}$	$2.16e^{-5}$	0.0002	0.0012

particle among all particles in the swarm is *Gbest*. Velocity and position of a particle are updated by the following update rules:

$$v_i(t)=\omega v_i(t-1)+\rho_1\frac{\left(x_{Pbest}-x_i(t)\right)}{\Delta t}+\rho_2\frac{\left(x_{Gbest}-x_i(t)\right)}{\Delta t} \quad (47)$$

$$x_i(t)=x_i(t-1)+v_i(t)\Delta t \quad (48)$$

Where ω is an inertia weight, Δt is the time-step value, ρ_1 and ρ_2 are random variables defined as $\rho_1=r_1c_1$ and $\rho_2=r_2c_2$ with $r_1,r_2\sim U(0,1)$, c_1, c_2 are positive acceleration constants. The time-step is necessary to make the algorithm dimensionally correct. The inertia weight ω is modified according to the following equation:

$$\omega=\omega_{\max}-\frac{\omega_{\max}-\omega_{\min}}{I_{tr\max}}I_{tr} \quad (49)$$

where, ω_{max} and ω_{min} are the initial and final inertia weights, I_{trmax} is the maximum number of iteration, and I_{tr} is the current number of iteration.

5.3 Adaptive-Network- based Fuzzy Inference System (ANFIS)

ANFIS is a class of adaptive multilayer feed-forward networks with the capability of using past samples to forecast the sample ahead [35]. The ANFIS network is comprised of five layers as shown in Fig. 8. Each layer includes several nodes described by the node function. Let Q_i^j denote the output of the i*th* node in layer *j*. In layer 1, every node is an adaptive node with node function

$$Q_i^1=\mu A_i(x), \qquad i=1,2 \quad (50)$$

$$Q_i^1=\mu B_{i-2}(y), \qquad i=3,4 \quad (51)$$

where, *x (or y)* is the input to the *ith* node and A_i (or B_{i-2}) is a linguistic label associated with this node. The membership functions for *A* and *B* are usually described by generalized bell functions.

$$\mu A_i(x)=\frac{1}{1+\left|\frac{x-r_i}{p_i}\right|^{2q_i}} \quad (52)$$

where, $\{p_i,q_i,r_i\}$is the parameter set. Parameters in this layer are referred to as premise parameters [35]. In layer 2, each node labeled $\prod$ multiplies incoming signals and sends the product out.

$$Q_i^2=\omega_i=\mu A_i(x)\mu B_i(y), \qquad i=1,2 \quad (53)$$

Each node output represents the firing strength of a rule. In layer 3, each *N* node computes the ratio of the *ith* rules' firing strength to the sum of all rules' firing strengths.

$$Q_i^3=\overline{\omega_i}=\frac{\omega_i}{\omega_1+\omega_2} \quad (54)$$

The outputs of this layer are called normalized firing strengths. In layer 4, each node computes the contribution of the *ith* rule to the overall output:

$$Q_i^4=\overline{\omega}_i z_i=\overline{\omega_i}(a_ix+b_iy+c_i), \quad i=1,2 \quad (55)$$

where, $\overline{\omega}_i$ is the output of layer 3 and $\{a_i,b_i,c_i\}$ is the parameter set. Parameters of this layer are referred to as consequent parameters. In layer 5, the single node $\sum$ computes the final output as the summation of all incoming signals.

$$Q_i^5=\sum_i\overline{\omega}_i z_i=\frac{\sum_i\omega_i z_i}{\sum_i\omega_i} \quad (56)$$

Thus, an adaptive network is functionally equivalent to a Sugeno-type fuzzy inference system.

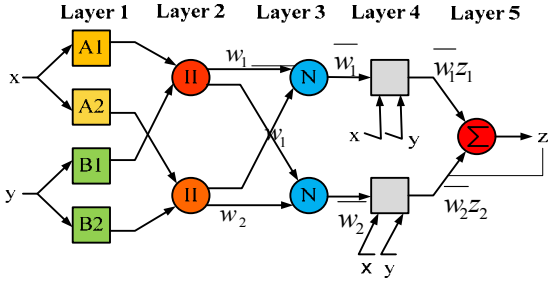

Fig.8. The ANFIS structure.

5.4 Hybrid approach

The structure of the proposed scheme is depicted in Fig. 9 and the implementation of it is described as following steps:

***First step*:** Form a matrix with a set of historical wind power with DFIG data (10 or 6 in this study), arranged in *C* columns of a matrix thereof.

Second step: Select a number of columns of the previous array so that the set of values derived from it represents the real input data. In addition, evaluate the fitness value of the initial group, which is given by:

$$F=\max\left\{\mathrm{Re}\,al(\lambda_1)\right\} \quad ,l=1,2,...,14 \quad (57)$$

Third step: The WT is used to decompose the input data. The decomposition is made from the choice of basic functions (58) (wavelet family of functions), and the number of levels wanted to split the series. The signal is divided into three levels: namely, a level of approximation (*A*) and details (*D*). The

wavelet function used is the Db4 type, which offers a good approach and ability to use a relatively small number of coefficients, making the code faster. Subsequently, in the level of decomposition, the detail series (for high frequencies) obtained is analyzed, so that they make a selection of coefficients in this series. This selection procedure is known as thresholding, because the purpose is to eliminate the coefficients smaller than a given value, with the aim of improving signal quality by removing noise. Finally, there is the process of reconstruction of the series.

Fourth step: Get the signal from the Wavelet, which can be submitted to the entrance of the ANFIS.

Fifth step: Train the ANFIS with the data obtained from the implementation of the previous step. The ANFIS uses a combination of the least-squares method (to determine consequent parameters) and the back propagation gradient descent method (to learn the premise parameters). The training process allows the system to adjust its parameters as inputs/outputs submitted [36]. The knowledge acquired through the learning process is tested by applying new data, called the testing set. The PSO is used to train the parameters within the membership functions of fuzzy inference system which leads to acquire more accurate results.

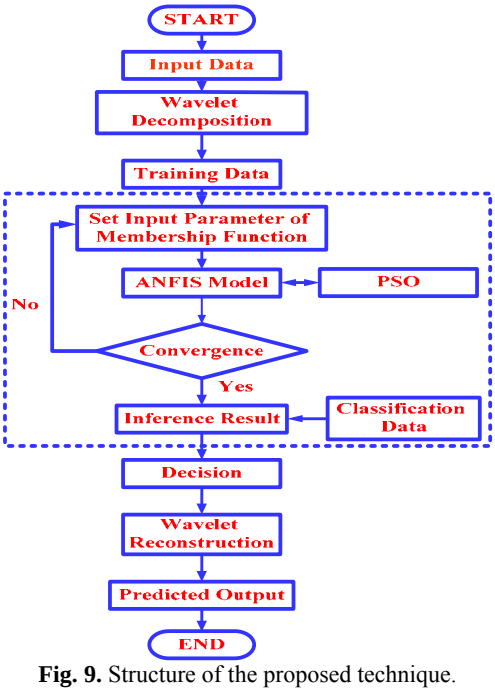

Fig. 9. Structure of the proposed technique.

Sixth step: Create a N-dimension vector, which will be optimized by PSO algorithm, where N is the number of membership functions. The fitness function is defined as the mean squared error.

Table 5. Parameters of PSO.

Parameters	C_1=0.2, C_2=0.2, ω_{min}=0.4, ω_{max}=0.9, Number of Particles=25, Number of Iterations=200

Table 6 shows the result of the three options. In addition, the results of the small signal stability analysis are tabulate in Table 7. As seen in the table, the similar result is achieved through optimizing the UDCP, related to the ten control parameters.

Table 6. Control parameters with and without optimization.

Option	Number of option			
	None	1	2	3
K_{p1}	1	1.1986	1.1992	1.0136
K_{i1}	100	80.032	79.693	98.874
K_{p2}	0.3	0.2541	0.2843	0.2849
K_{i2}	8	4.986	5.023	8.066
K_{p3}	1.25	10.530	1.231	1.1961
K_{i3}	300	220.02	220.82	325.95
K_{pdg}	0.002	0.0123	0.0136	0.0028
K_{idg}	0.05	0.0521	0.046	0.0536
K_{pg}	1	0.7251	0.7526	0.8266
K_{ig}	100	129.56	100.6	98.685

6. SIMULATION RESULTS

In this case, two different power system, single machine infinite-bus system and multi-machine power system are applied to confirm the improvement in dynamic stability by the controller of the WT with DFIG system with the optimized UDCP control parameters.

Case 1: SMIB with small disturbance

The small disturbance is set as the DFIG voltage reference decrease from 1.0 pu to 0.9 pu. The dynamics of the active power, reactive power and dc link voltage are shown in Figs. 10-12, respectively. Each of these figures show four curves with different parameters: the original control parameters optimized all control parameters, optimized random six control parameters and optimized UDCP.

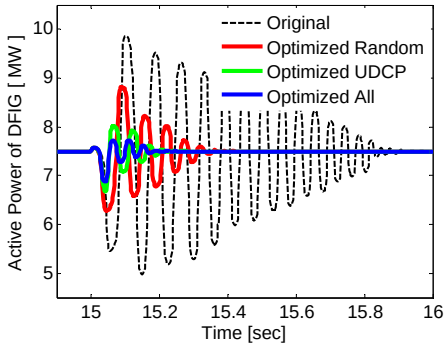

Fig. 10. Active power of SIMB under small disturbance.

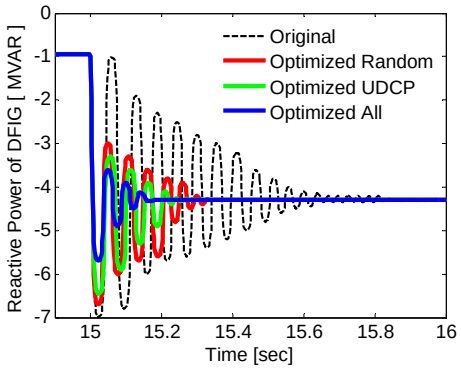

Fig. 11. Reactive power of SMIB under small disturbance.

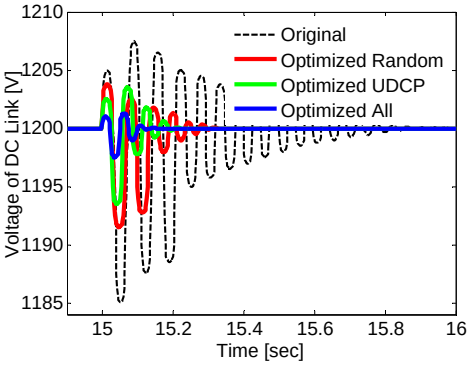

Fig. 12. Voltage of dc link of SMIB under small.

As seen, the dynamic performance of the DFIG base WT using the optimized UDCP is nearly the same as using all the ten optimized control parameters. According to the figures following results are achieved: significant reduction in the magnitudes of the active power, reactive power, voltage sag and overshoot; better oscillation damping with the optimized UDCP than that with_out the optimization. In addition, although the performance of optimized random six control parameters is better than the original one, it cannot compete with the proposed approach with the optimized UDCP.

Case 2: SMIB with large disturbance

In this case, a three-phase ground fault in the middle of the transmission line is applied at t=15 s, and cleared after 0.15 s. Figures 13-15 illustrate the dynamics of the active power, output reactive power and dc link voltage.

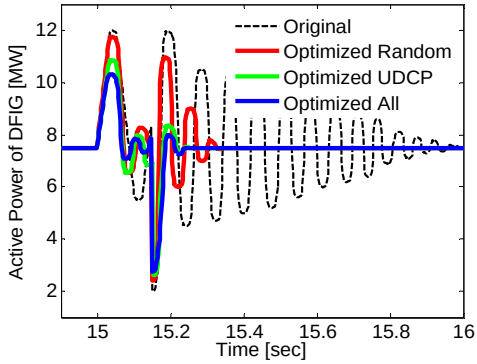

Fig. 13. Active power of SMIB under small disturbance.

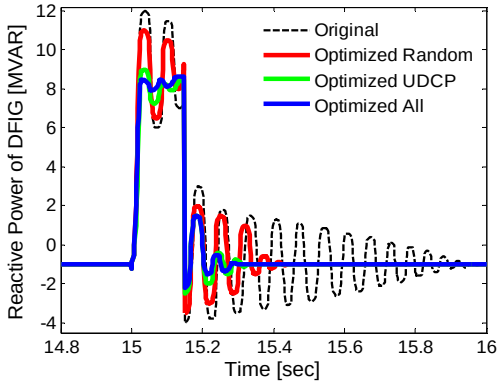

Fig. 14. Reactive power of SMIB under small disturbance.

The oscillation after the disturbance is damped out very quickly as similar as in the small disturbance in case 1. Therefore, the optimized UDCP enhances the fault ride through capability of the WT system.

Table 7. Eigenvalue analysis with different options disturbance.

Option		λ_1	λ_2	$\lambda_{3,4}$	$\lambda_{5,6}$	$\lambda_{7,8}$	λ_9	$\lambda_{10,11}$	λ_{12}	λ_{13}	λ_{14}
1	σ	-66952	-198	-89.53	-111.2	-3.52	-52	-0.46	-4.65	-17.85	-18.22
	ω	0	0	78	57	61.5	0	0.55	0	0	0
2	σ	-66676	-154.2	-98.65	-3.56	-98.41	-47.6	-0.56	-4.22	-17	-17.31
	ω	0	0	98.26	61	54.67	0	0.55	0	0	0
3	σ	-11225	-175.2	-84	-102	-2.56	-84.26	-.55	-25	-26	-17
	ω	0	0	115.2	50.23	63	0	0.53	0	0	0

In addition, as seen in these figures, the performance of optimized random six control parameters is not as good as optimized UDCP.

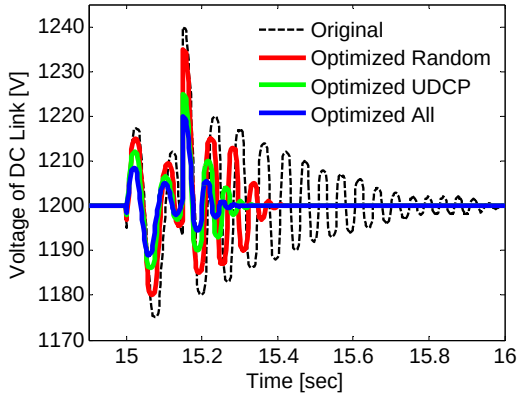

Fig. 15. Voltage of dc link of SIMB under small.

Case 3: Multi-machine power system

A multi-machine power system is also used to verify the strong performance of the proposed scheme.

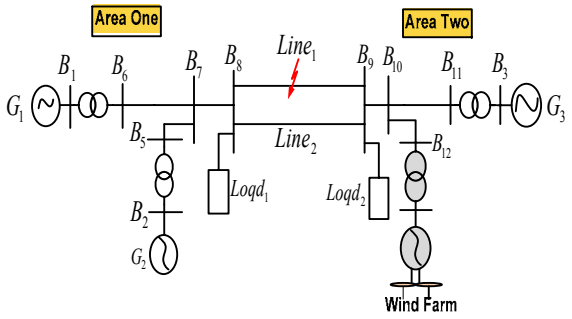

Fig.16. Schematic diagram of the multi-machine power system with DFIG.

The system is divided into two areas, in each of which there are two machines. In addition, the four-machine-two-area system is modified by replacing generator G4 with a DFIG, which is the same as that used in the above SMIB power system. The DFIG capacity is 36 MW as indicated in Section 2, where the other three synchronous machines have the same capacity as the DFIG. Before the fault occurs, the active power transfers from area one to area two is almost 15 MW [37]. Hence, a single-phase ground fault is applied (see Fig. 16) at the t=30 s, and cleared after 0.2 s without tripping the line. The dynamics of the active power, voltage of the DFIG and dc link voltage are shown in Figs. 17–19.

As shown, the dynamic performance of the DFIG based WT using the optimized UDCP is better than the optimized random six control parameters. In addition, damping the oscillation after the disturbance is as quickly as in the SMIB power system. The dynamic responses of generator 3 (G3) will be affected significantly owing to its nearness to the DFIG. The oscillation of the voltage of G3 is damped quickly as shown in Figure 20. Figure 21 shows the convergence of cost function. According to the figure, the convergence of training error of the PSO-ANFIS is meaningfully fast.

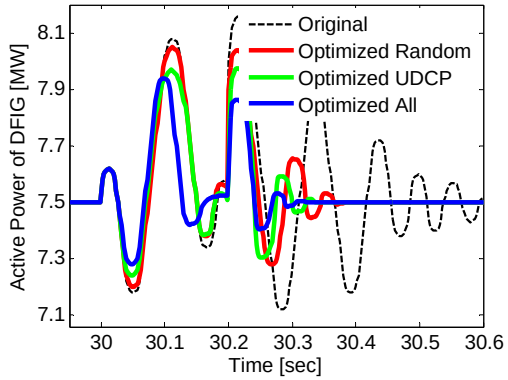

Fig. 17. Active power of the WT with DFIG in multi-machine power system.

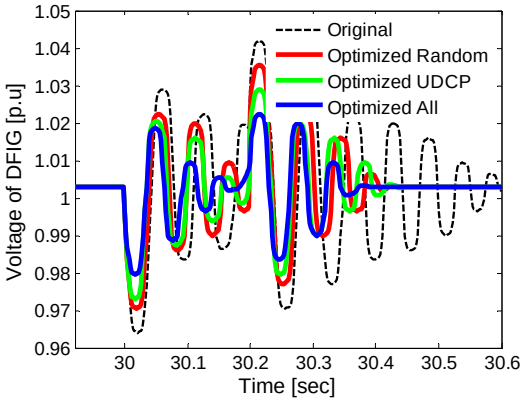

Fig. 18. Voltage of the WT with DFIG in multi-machine power system.

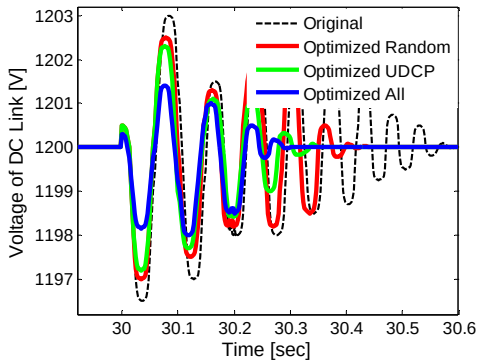

Fig. 19. Voltage of dc link in multi-machine power system.

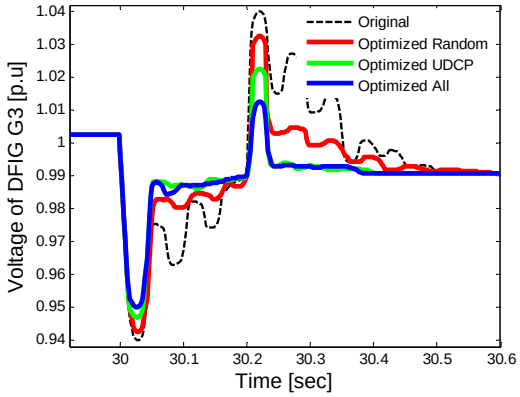

Fig. 20. Voltage of G3 in multi-machine power system.

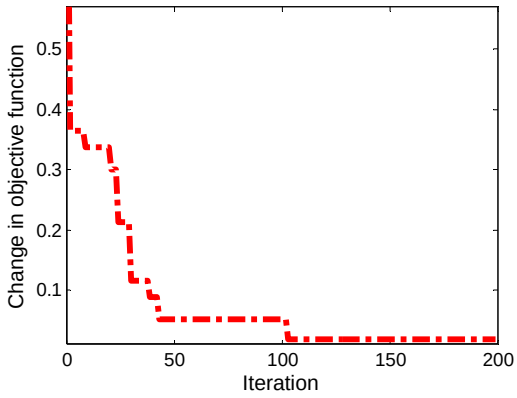

Fig. 21. Training error of the PSO-ANFIS.

7. CONCLUSIONS

A DFIG wind turbine model containing drive train, pitch control, induction generator, back-to-back PWM converters, RSC, GSC and vector-control loops is developed in this paper. A sensitivity analysis based on trajectory sensitivity and eigenvalue sensitivity analysis is performed on the DFIG control parameters to choose the unified dominate control parameters. A novel hybrid approach is applied to find the optimal control parameters in order to acquire the optimal control of the multiple controllers of the wind turbine system. The proposed approach is based on the combination of wavelet transform, particle swarm optimization, and an adaptive-network-based fuzzy inference system. The wavelet transform is used to decompose the wind power series into a set of better-behaved constitutive series. Then, the future values of these constitutive series are estimated using ANFIS. The PSO is employed to improve the performance of ANFIS to obtain a lower error. The main advantages of the proposed approach are concluded as follow:

- Reduction in computational cost due to decrement of selected UDCP parameters via sensitivity analysis;
- Significant reduction in the magnitudes of the active power, reactive power, voltage sag and overshoot, and consequently improving dynamic performance of the WT system;
- Better oscillation damping with the optimized UDCP;
- Reduction in computational time compared with the case of optimizing all control parameters, which leads to improve the optimization efficiency;

REFERENCES

[1] J. P. S. Catalão, H. M. I. Pousinho, and V. M. F. Mendes, "Hybrid wavelet-PSO-ANFIS approach for short-term wind power forecasting in portugal," *IEEE Transaction on Sustainable Energy* , vol. 2, no. 1, pp. 50-59, 2011.

[2] Z. Li, J. B. Park, Y. H. Joo, B. Zhang and G. R.Chen, "Bifurcation and chaos in a permanent-magnet synchronous motor," *IEEE Transaction on Circuits System Fundamental Theory and Application*., vol. 49, no. 3, pp. 383–387, 2002.

[3] Y. Gao and K. T. Chau, "Hopf bifurcation and chaos in synchronous reluctance motor drives," *IEEE Transaction on Energy Conversion.*, vol. 19, no. 2, pp. 296–302,Jun 2004.

[4] K. E. casey, B.F. Hobbs, D. Shirmohammadi and F.A. Wolak, "Benefit cost analysis of large-scale transmission for renewable generation: principles & California case study," *Proc. Of the IEEE Power Engineering Society General Meeting*, pp. 1–3, June 2007.

[5] G.B. Shrestha and P.A.J. Fonseka, "Congestion-driven transmission expansion in competitive power markets," *IEEE Transaction on Power System*., vol. 19, no. 3, pp. 1658–1665, 2004.

[6] S. Grijalva and A. M. Visnesky, "The effect of generation on network security: spatial representation, metrics, and policy," *IEEE Transaction on Power System*, vol. 21, no. 3, pp. 1388–1395, 2006.

[7] P. Pinson, S. Lozano, I. Marti, G. N. Kariniotakis, and G. Giebel, "ViLab: A virtual laboratory for

collaborative research on wind power forecasting," *Wind Energy*, vol. 31, no. 2, pp. 117–122, Mar. 2007.

[8] N. Cutler, M. Kay, K. Jacka and T. S. Nielsen, "Detecting, categorizing and forecasting large romps in wind farm power output using meteorological observations and WPPT," *Wind Energy*, vol. 10, no. 5, pp. 453-470, 2007.

[9] H. Aa Nielsen, T. S. Nielsen, H. Madsen, M. J. S. I. Pindado and I. Marti, "Optimal combination of wind power forecasts," *Wind Energy*, vol. 10, no. 5, pp. 471-482, 2007.

[10] P. Pinson, H. A. Nielsen, J. K. Moller, H. Madsen, and G. N. Kariniotakis, "Non-parametric probabilistic forecasts of wind power: Required properties and evaluation," *Wind Energy*, vol. 10, no. 6, pp. 497–516, 2007.

[11] L. Yang, G. Y. Yang, Z. Xu, Z. Y. Dong, K. P. Wong, and X. Ma, "Optimal controller design of a doubly-fed induction generator wind turbine system for small signal stability enhancement," *IET Proceedings on Generation, Transmission and Distribution*., vol. 5, pp. 579–597, 2010.

[12] W. Qiao, J. Liang, G. K. Venayagamoorthy, and R. G. Harley, "Computational intelligence for control of wind turbine generators," *Proc. Of the IEEE Power Energy Society General Meeting*, pp. 6, 2011.

[13] A. Mendonca and J. A. P. Lopes, "Robust tuning of power system stabilizers to install in wind energy conversion systems," *IET Renewable Power Generation*, vol. 3, no. 4, pp. 465–475, 2009.

[14] N. Kshatriya, U. D. Annakkage, F. M. Hughes, and A. M. Gole, "Optimized partial eigenstructure assignment-based design of a combined PSS and active damping controller for a DFIG," *IEEE Transaction on Power System.*, vol. 25, no. 2, pp. 866–876, 2010.

[15] H. Huang and C. Y. Chung, "Coordinated damping control design for DFIG-based wind generation considering power output variation," *IEEE Transaction on Power Systems*, vol. 27, no. 4, pp. 1916–1925, 2012.

[16] F.Wu, X. P. Zhang, K. Godferey and P. Ju, "Small signal stability analysis and optimal control of a wind turbine with doubly fed induction generator," *IET Proceedings on Generation, Transmission and Distribution*, vol. 1, pp. 751–760, 2007.

[17] P. J. Werbos, "Computational intelligence for the smart grid-history, challenges, and opportunities," *IEEE Computational Intelligence Magazine*, vol.6, no. 3, pp. 14–21, 2011.

[18] G. K. Venayagamoorthy, "Dynamic, stochastic, computational, and scalable technologies for smart grids," *IEEE Computational Intelligence Magazine*, vol. 6, no. 3, pp. 22–35, 2011.

[19] W. Qiao, R. G. Harley and G.K. Venayagamoorthy," Coordinated reactive power control of a large wind farm and a STATCOM using heuristic dynamic programming," *IEEE Transaction on Energy Conversion*., vol.24, no. 2, pp. 493–503, 2009.

[20] W. Qiao, G. K. Venayagamoorthy and R. G. Harley, "Real-time implementation of a STATCOM on a wind farm equipped with doubly fed induction generators," *IEEE Transaction on Industry Applications*, vol. 45, no. 1, pp. 98–107, Jan./Feb. 2009.

[21] H. L. Xie, P. Ju, J. Luo, Y. Ning, H. Zhu and X.Wang, "Identifiability analysis of load parameters based on sensitivity calculation," *Automation Electric and Power System.*, vol. 33, pp. 17–21, 2009.

[22] L. H. Yang, Z. Xu, J. Østergaard, Z. Y. Dong, K. P .Wong, and X. Ma, "Oscillatory stability and eigenvalue sensitivity analysis of a DFIG wind turbine system," *IEEE Transaction on Energy Conversion*, vol. 26, pp. 328–339, 2011.

[23] R. Aghatehrani and R. Kavasseri, "Reactive power management of a DFIG wind system in micro-grids based on voltage sensitivity analysis," *IEEE Transaction on Sustainable Energy*, vol. 2, pp. 451–458, 2010.

[24] A. D. Hansen, P. Sørensen, F. Iov and F. Blaabjerg, "Control of variable speed wind turbines with doubly-fed induction generators," *Wind Energy*., vol. 28, no. 4, pp. 411–434, 2004.

[25] A. D. Hansen, P. Sørensen, F. Iov and F. Blaabjerg, "Control of variable speed wind turbines with doubly-fed induction generators," *Wind Energy*., vol. 28, no. 4, pp. 411–434, 2004.

[26] L. Rouco and J. L. Zamora, "Dynamic patterns and model order reduction in small-signal models of doubly fed induction generators for wind power applications," *Proc. Of the IEEE Power Engineering Society General Meeting*, pp. 1-8, 2006.

[27] P. C. Krause, O. Wasynczuk, and S. D. Sudhoff, "*Analysis of electric machinery and drive systems. piscataway*, " NJ: *IEEE Press*, 2002.

[28] P. Juand and D.Q. Ma, "*Identification of power load*," 2nd ed. Beijing, China: China Electric Power Press, 2008.

[29] Y.Tang, P.Ju, H. He, C. Qin and F. Wu, Optimized control of DFIG-based wind generation using sensitivity analysis and particle swarm optimization", *IEEE Transaction on smart grid*, vol. 4, no. 1, 2013.

[30] N. Amjady and F. Keynia, "Short-term load forecasting of power systems by combination of wavelet transform and neuro-evolutionary algorithm," *Energy*, vol. 34, no. 1, pp. 46–57, 2009.

[31] A. J. R. Reis and A. P. A. da Silva, "Feature extraction via multi-resolution analysis for short-term load forecasting," *IEEE Transaction on Power System*, vol. 20, no. 1, pp. 189–198, 2005.

[32] Z. A. Bashir and M. E. El-Hawary, "Applying wavelets to short-term load forecasting using PSO-based neural networks," *IEEE Transaction on Power Systems*, vol. 24, no. 1, pp. 20–27, 2009.

[33] W. Yu and X. Li, "Fuzzy identification using fuzzy neural networks with stable learning algorithms," *IEEE Transaction on Fuzzy Systems*, vol. 12, pp. 411–420, 2004.

[34] J. S. Heo, K. Y. Lee, and R. Garduno-Ramirez, "Multi-objective control of power plants using particle swarm optimization techniques," *IEEE Transaction on Energy Conversion*, vol. 21, pp. 552–561, 2006.

[35] Z. Yun, Z. Quan, S. Caixin, L. Shaolan, L. Yuming, and S. Yang, "RBF neural network and ANFIS-based short-termload forecasting approach in real-time price environment," *IEEE Transaction on Power System*, vol. 23, no.3, pp. 853-858, 2008.

[36] J. -S. R. Jang, "ANFIS: Adaptive-network-based fuzzy inference system," *IEEE Transaction on Power Systems*, vol. 23, no. 3, pp. 665-685, 1993.

[37] F.Wu, X. P. Zhang, P. Ju, and M. J. H. Sterling, "Decentralized nonlinear control of wind turbine with doubly fed induction generator," *IEEE Transaction on Power Systems*, vol. 23, no. 2, pp. 613-621, 2008.